ACS APPLIED MATERIALS & INTERFACES

Letter

www.acsami.org

Multilayer Graphitic Coatings for Thermal Stabilization of Metallic Nanostructures

Peter M. Wilson,[†] Adam Zobel,[†] Alexey Lipatov,[†] Eva Schubert,[‡,§] Tino Hofmann,[‡,§] and Alexander Sinitskii*[,†,§]

[†]Department of Chemistry, [‡]Department of Electrical Engineering, and [§]Nebraska Center for Materials and Nanoscience, University of Nebraska—Lincoln, Lincoln, Nebraska 68588, United States

Supporting Information

ABSTRACT: We demonstrate that graphitic coatings, which consist of multilayer disordered graphene sheets, can be used for the thermal protection of delicate metal nanostructures. We studied cobalt slanted nanopillars grown by glancing angle deposition that were shown to melt at temperatures much lower than the melting point of bulk cobalt. After graphitic coatings were conformally grown over the surfaces of Co nanopillars by chemical vapor deposition, the resulting carbon-coated Co nanostructures retained their morphology at elevated temperatures, which would damage the uncoated structures. Thermal stabilization is also demonstrated for carbon-coated Ti nanopillars. The results of this study may be extended to other metallic and possibly even nonmetallic nanostructures that need to preserve their morphology at elevated temperatures in a broad range of applications.

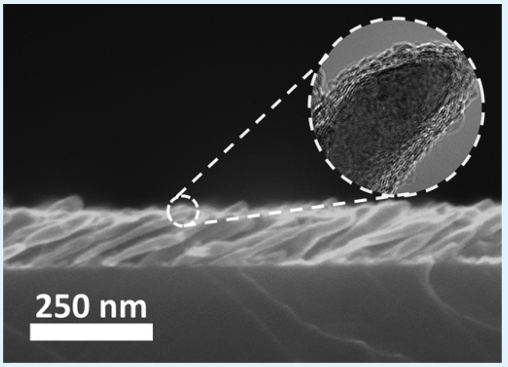

KEYWORDS: *chemical vapor deposition, graphene, thermal stabilization, glancing angle deposition, HR-TEM, thin films*

Graphene, a two-dimensional (2D) carbon allotrope, has a number of technologically relevant properties that include very high electronic[1−3] and thermal[4] conductivities, great mechanical properties,[5] optical transparency,[6] impermeability to gases,[7] as well as other unique characteristics.[8] These properties make graphene a very promising material for numerous future applications across the technological spectrum.[9] Some of the commonly discussed electronics applications of graphene include high-frequency transistors,[10,11] transparent conductive electrodes for solar cells,[12] touch screens[13] and flexible organic light-emitting diodes,[14] gas sensors,[15,16] and energy storage devices.[17,18] Exceptional mechanical properties of graphene can find use, for example, in electromechanical resonators,[19] transmission electron microscopy (TEM) supports,[20] and transparent impermeable windows in liquid cells for in situ microscopic[21,22] and spectroscopic[23] characterization of materials. Graphene's mechanical properties, impermeability to molecules, and chemical inertness justify its use as a corrosion-resistant coating for protection of metals from oxidative degradation.[24,25] A great advantage of graphene for the corrosion protection of metals is the fact that graphene can be conformally grown on complex 2D and even three-dimensional (3D) metallic substrates by chemical vapor deposition (CVD) method.[26−29] In this Letter, we demonstrate a related but another potential application of graphene—we show that conformal graphene coatings can be used for the thermal protection of delicate metal nanostructures, making them resistant to melting at increased temperatures.

Providing metallic nanostructures with thermal stability, the ability to withstand increased temperatures without suffering morphological deformation, has been a recent challenge in the field of nanotechnology. In general, materials with decreased dimensions have decreased thermal stability and will melt at lower temperatures than their bulk counterparts as described by the Gibbs−Thomson effect.[30−32] This decrease in thermal stability of the metal nanoparticles can cause them to melt and coalesce into much larger and less useful materials, having lost the interesting properties afforded by their nanoscopic size. Thus, technological implementation of nanomaterials has generally been limited in high temperature applications, such as catalysis, by the thermal instability of nanoscopic materials.

The challenge of stabilizing nanostructures to make them useful at increased temperatures has driven many investigations into various methods of making nanoparticles more resistant to thermal damage. Such methods include bimetallic alloying,[33,34] encapsulation in inert oxide coating,[30] utilizing a carbon nanotube nanoreactor,[35] coating in a mesoporous silica shell,[36] and others.[37] Thus, finding a method to stabilize nanostructures and make them resistant to melting is of significant technological interest.

As a test object for this study, we have selected slanted columnar thin films (SCTFs) that are schematically shown in Figure 1. Top- and side-view scanning electron microscopy

Received: October 1, 2014
Accepted: January 16, 2015
Published: January 16, 2015

DOI: 10.1021/am506777a
ACS Appl. Mater. Interfaces 2015, 7, 2987−2992

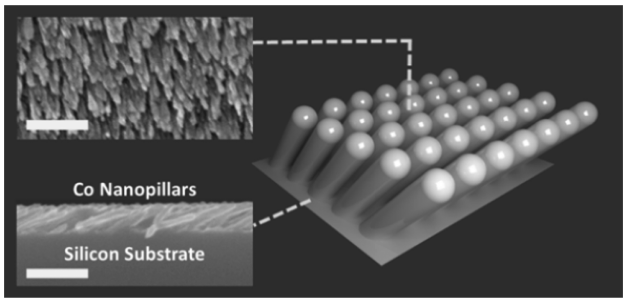

Figure 1. 3D schematic of slanted columnar thin films (SCTFs). Top-view and cross-section SEM images of cobalt SCTFs, which were used in this study, are shown in the top and bottom insets, respectively. Scale bars are 250 nm.

(SEM) images (see the insets in Figure 1) of a cobalt SCTF show that it is composed of a dense array of slanted Co nanopillars grown by glancing angle deposition (GLAD) method.[38] Technologically, SCTFs are relevant for a number of potential applications that include optical humidity detectors,[39] pressure sensors,[40] and gas sensors.[41] Increased thermal stability of these structures would increase the range of conditions under which they could be used, and open up multitudes of treatments to modify the nanostructures.

SCTFs are a class of materials that are especially susceptible to thermal damage because of the nanoscopic dimensions of slanted pillars. Additionally, these nanopillars are highly polycrystalline, resulting in even greater thermal instability. In the case of cobalt SCTFs that have been used in this study, our preliminary experiments showed that Co SCTFs were damaged if annealed at the relatively low temperature of 500 °C, which is much lower than the melting point of bulk Co (1495 °C) as shown in Figure S1 in the Supporting Information.

With recent advances in CVD techniques, graphene can be conformally grown on complex 2D and 3D metallic substrates.[26−29] In this study, we demonstrate that graphitic coatings can be grown over the surface of delicate SCTFs that consist of slanted polycrystalline cobalt nanopillars. These conformal graphitic coatings can increase the thermal stability of the Co nanostructures. The remarkably increased melting resistance enables the nanopillars to remain in a near-pristine morphology at elevated temperatures for lengthy periods of time at which the bare SCTFs would be significantly deformed.

Cobalt nanopillar arrays were grown by e-beam evaporation of Co at an angle of 85° on the surface of a silicon substrate. A detailed growth procedure is given elsewhere.[42] Figure 2a shows a cross-section SEM image of a typical Co SCTF sample used in this study. SEM images were taken using a Hitachi S4700 field-emission scanning electron microscope. Annealing the cobalt SCTFs at 500 °C for 10 min resulted in highly deformed structures as shown in Figure 2b. In the process of annealing, the nanopillars melted together, forming significantly wider structures while still retaining a generally slanted morphology. However, the nanopillars were no longer uniformally slanted but had a range of different slanting angles. Because the slanted pillarlike morphology is retained and the pillars do not coalesce into round droplets, it is likely that this deformation is due to the formation of a "liquid skin" that encapsulates a solid core. This liquid skin model has previously been used to accurately describe the melting behavior of aluminum nanoparticles.[43]

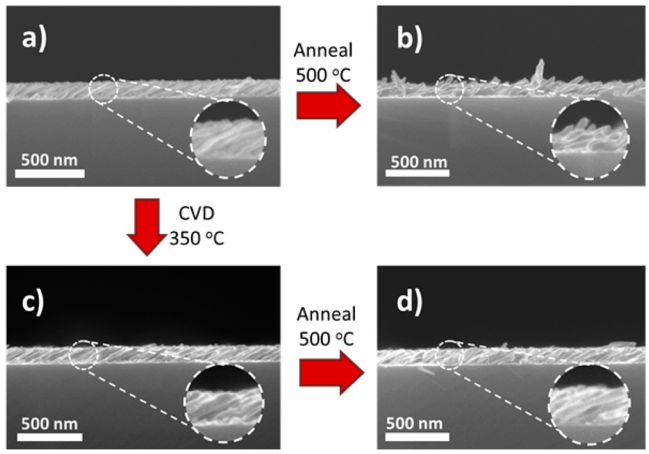

Figure 2. Cross-section SEM images of cobalt SCTFs: (a) as-grown, (b) annealed, (c) graphene-coated, and (d) annealed after graphene coating.

These results show that in order to conformally cover Co SCTFs with graphene, the temperature of the CVD graphene growth should be below 500 °C. Typical CVD procedures employ a methane precursor and raise the temperature to 1000 °C at which Co slanted nanopillars will be damaged. To accommodate the low-temperature restriction, we used acetylene as a hydrocarbon source instead of methane because of acetylene's higher reactivity.[29,44,45] The CVD coating of the SCTFs was performed by heating a tube furnace to a temperature of 350 °C under hydrogen. Under such conditions, the SCTFs suffer very little damage. The details of CVD experiments are given in the Supporting Information. The resulting product was a well-preserved uniform SCTF in which the nanopillars retain their morphology, as can be seen in Figure 2c. The samples were studied by Raman spectroscopy using a Thermo Scientific DXR Raman microscope. The Raman spectrum of carbon-coated SCTFs showed a disordered graphene product by the presence of wide, conjoined and asymmetric D and G bands and by the absence of a 2D band (not shown). Despite the fact that this carbon coating is not composed of perfect mono- or few-layer graphene sheets, it has a dramatic effect on the thermal stability of Co nanostructures. When the carbon-coated Co SCTFs were annealed at 500 °C under H_2/Ar for 10 min, they did not show any noticeable degradation, as the morphology and the slanting angle of nanopillars remained nearly the same (Figure 2d), in stark contrast to bare cobalt SCTFs, which were significantly altered when similarly annealed (Figure 2b).

The microstructure of the graphitic coating was studied by transmission electron microscopy (TEM) using a FEI Tecnai Osiris transmission electron microscope. Representative TEM images of two carbon-coated Co nanopillars are shown in Figure 3. These images show that the CVD-grown graphitic coatings are conformal, continuous and typically have a thickness of 5−10 graphene layers. These coatings improve the mechanical and thermal stability of Co nanopillars and allow them to retain their morphology well when annealed at 500 °C.

Mueller matrix ellipsometry (MME), which measures changes in the polarization of light upon interaction with a surface (Figure 4a), has been shown to be a powerful tool for characterizing the SCTF's properties.[46] in particular, MME has been shown to be very sensitive to quantifying the presence of

DOI: 10.1021/am506777a
ACS Appl. Mater. Interfaces 2015, 7, 2987−2992

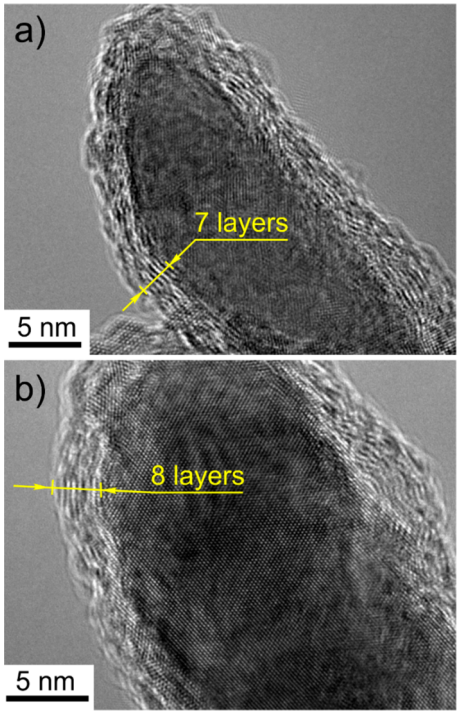

Figure 3. (a, b) TEM images of the disordered graphene product grown by CVD over the surface of the cobalt nanopillars.

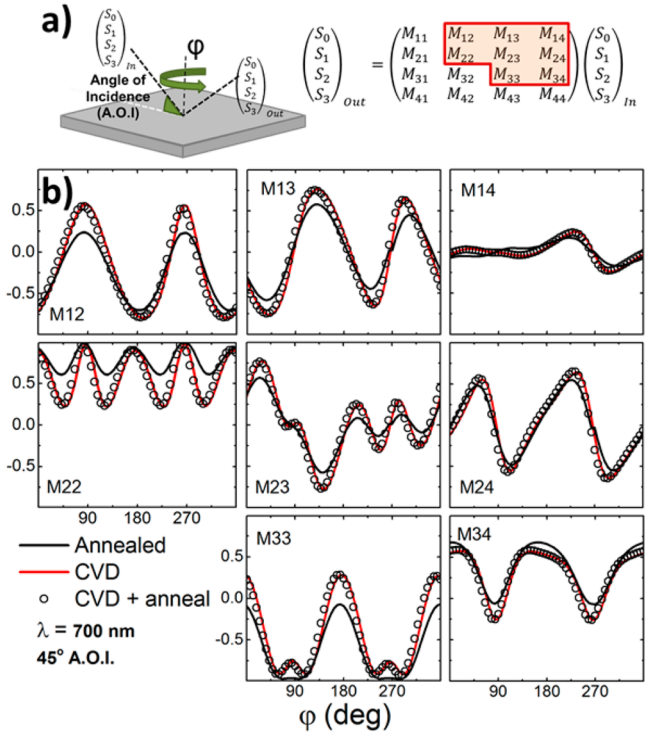

Figure 4. (a) Schematic showing how changes in polarization states (S_i) are calculated using the Mueller matrix and measured as a function of azimuth φ; Mueller matrix elements which are displayed are highlighted in orange. (b) MME data for annealed (black line), carbon-coated (red line), and carbon-coated and then annealed (empty circles) Co SCTFs.

adsorbates on SCTFs and for monitoring the structural morphology of the SCTFs when it is measured as a function of the azimuth (φ),[29,42] and therefore is a suitable technique for observing changes to the sample after annealing. Unlike SEM that could be used to observe the morphology of SCTFs on a micrometer scale, MME collects a signal that is averaged for a ~ 1 × 1 cm^2 SCTF area. Therefore, SEM and MME data complement each other providing structural information about SCTFs at different scales.

MME measurements of SCTFs at λ = 700 nm and the angle of incidence (A.O.I.) of 45° were performed using a J.A. Woollam M2000 instrument with a rotating stage. The results of the MME measurements of annealed (Figure 2b) and carbon-coated Co SCTFs (Figure 2c), as well as Co SCTFs that were carbon-coated and then annealed (Figure 2d) are shown in Figure 4b. Because of their slanted structure, carbon-coated SCTFs exhibit an anisotropic optical response that strongly depends on φ (Figure 4b). The Mueller matrix spectra of carbon-coated SCTFs are nearly identical to the spectra of annealed carbon-coated SCTFs, suggesting that the average slanting angle and the morphology of carbon-coated Co nanopillars do not change upon annealing at 500 °C. Although the same conclusion was made based on the local SEM observations (Figure 2), MME data further confirm the thermal stability of carbon-coated SCTFs on a centimeter scale. In contrast, the MME spectra of the as-grown SCTFs change substantially during the annealing at 500 °C (Figure 4b). In particular, the decreased amplitude of the signal change as a function of φ suggests the decreased anisotropy caused by the higher degree of disorder in annealed Co SCTF sample, which was also observed in the cross-section SEM images (Figure 2).

To test the thermal stability of the carbon-coated SCTFs, we annealed the substrates at 500, 600, and 700 °C in three separate experiments under an Ar/H_2 environment for 10 min. As the annealing temperature increased, more thermal damage was induced on the nanostructures. The damaged pillars tended to coalesce into structures with lower aspect ratios due to the spherification that occurs upon melting. However, as shown by the SEM images (Figure 5), only certain regions of the SCTFs appeared damaged by the high temperatures, whereas many of the nanopillars appeared to retain their original morphology and packing density. To characterize the types of pillars that would be thermally protected and those that would be damaged, the width distribution of the nanopillars was measured using top-view SEM images (Figure 5a), according to the following rules: only the tips of the pillars were measured, if the tips were obscured they were not counted, each pillar was measured once, damaged nanostructures (those with aspect ratios of less than 2:1 or widths of greater than 100 nm) were not counted. Representative SEM images that were used for measuring size distributions of the nanopillars are shown in Figure S2 in the Supporting Information; a sample size of 100 counts was measured for each of the various samples.

As expected, the width distributions of the carbon-coated SCTFs before and after annealing at 500 °C were similar and had similar average widths of 39 and 40 nm, respectively. Interestingly, the pillars that remained undamaged at the higher temperatures tended to be narrower, with the 600 °C annealing giving average widths of 34 nm, and the 700 °C annealing resulting in an average width of 31 nm. This implies that the larger nanopillars were more susceptible to damage, and had a greater tendency to coalesce into the larger globules. This appears to be in contradiction to the Gibbs−Thomson equation for melting point depression of small particles,

DOI: 10.1021/am506777a
ACS Appl. Mater. Interfaces 2015, 7, 2987−2992

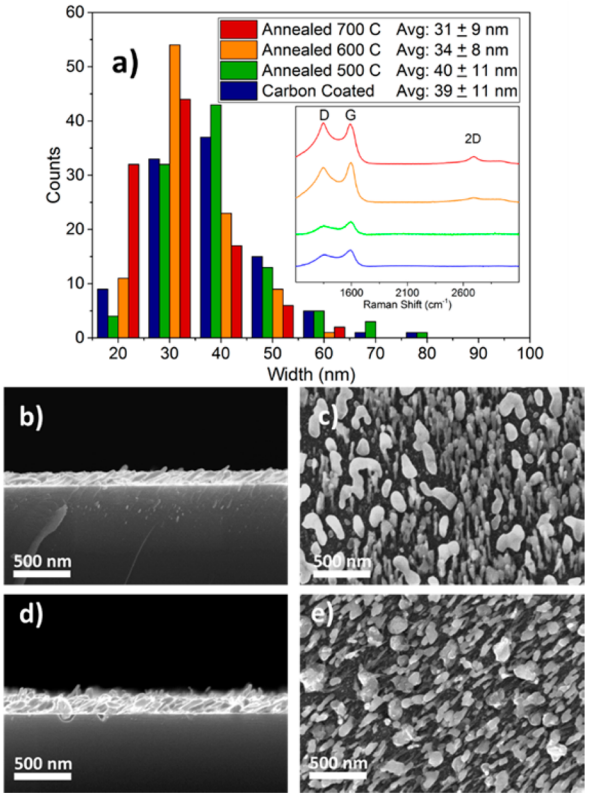

Figure 5. (a) Width distributions of as-grown carbon-coated Co nanopillars and the samples after annealing at 500, 600, and 700 °C. Only undamaged nanopillars with aspect ratios of more than 2:1 and widths of smaller than 100 nm were counted. Inset shows the evolution of Raman spectra upon annealing at different temperatures. (b, c) SEM images of carbon-coated Co nanopillars after annealing at 600 °C: (b) side view and (c) top view. (d, e) SEM images of carbon-coated Co nanopillars after annealing at 700 °C: (d) side view and (e) top view.

which states that structures with the smaller dimensions ought to be the first to suffer thermal damage.

There are several possible reasons for this trend. One possible reason for this could be the ease of dissolution of carbon into the larger pillars compared with the thinner pillars. Graphene growth on cobalt occurs by the subsequent dissolution and precipitation of carbon from the cobalt.[44] Because the larger pillars have a smaller surface-to-volume ratio, by extension there is also a lower carbon to cobalt ratio, making it easier for the carbon coating to be fully dissolved within the nanopillar resulting in loss of the insulative coating. This hypothesis appears consistent with the Raman data shown in the inset in Figure 5a. After dissolution within the nanopillars, the carbon then segregates to the surface of the nanopillars upon cooling forming a more graphene-like product. Raman analysis of the annealed nanopillars shows the emergence of a signal in the 2D-band region around 2700 cm^{-1}, a characteristic band of graphite and graphene-like carbon. This peak is sharper and more defined in the sample which had been annealed at 700 °C, indicating that more graphitic product had been formed. It should be noted, therefore, that the graphene coating can only provide the thermal protection at conditions that will not result in the complete dissolution of the carbon into the bulk of the nanostructures.

Furthermore, we tested the extents to which the thermal stabilization will take effect and whether the protective coating can be grown under different conditions. To this end, we exposed cobalt SCTFs to C_2H_2 and H_2 while the temperature was raised to 400 °C. After CVD growth, the resulting carbon-coated nanostructures were annealed under H_2/Ar for 2 h. As shown by SEM in Figure S3 in the Supporting Information, the nanopillars remained well-preserved, having high nanopillar density and retaining uniform slanting angles and nanopillar height. This demonstrates that the CVD procedure to produce a protective coating is not particularly demanding and that the thermal stability persists for extended lengths of time.

Finally, in order to determine whether the thermal stabilization is a general property of the amorphous carbon coating, or if it is specific to the cobalt−carbon system, we used SCTFs made from titanium as another test case. Because titanium has greatly different physical and chemical properties from cobalt, the procedure was modified to be suitable to titanium as follows. Because Ti has significantly poorer catalytic properties than Co, CVD was performed at 500 °C with C_2H_2 and H_2. Additionally, the Ti SCTFs were shown to be much more resistant to melting, and only showed signs of melting when annealed under H_2/Ar at 800 °C for 10 min. However, as shown by SEM images in Figure 6, the carbon-coated Ti

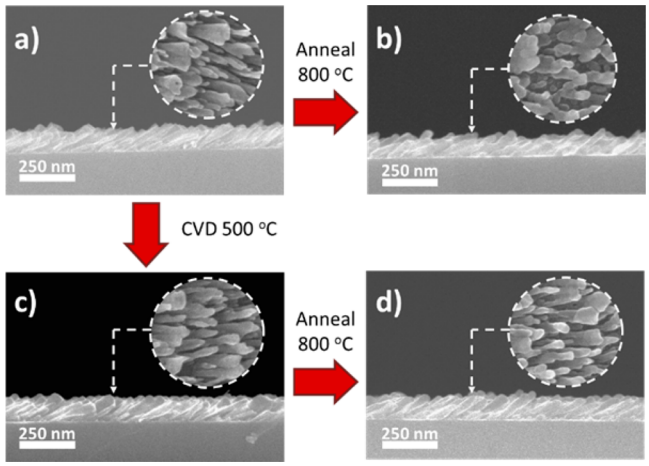

Figure 6. Cross-section and top-view (insets) SEM images of (a) as-grown, (b) annealed at 800 °C, (c) CVD-coated, and (d) CVD-coated and annealed Ti SCTFs.

SCTFs were able to withstand the 10 min annealing under H_2/Ar at 800 °C far better than the bare nanopillars were. This demonstrates that the carbon coating is able to provide thermal stabilization to materials with very different physical and chemical properties.

In summary, we have shown that conformal carbon coatings can be used for the thermal protection of delicate metal nanostructures, making them resistant to melting at increased temperatures. In addition, we expect that upon graphene coating, otherwise fragile nanostructures would be both mechanically,[47] and chemically stabilized.[24,25] As a test object for this study, we used Co SCTFs that are very susceptible to thermal damage due to the nanoscopic dimensions and polycrystallinity of slanted Co nanopillars. Conformal graphitic coatings were grown on the surface of Co SCTFs by CVD at 350 °C using acetylene as a carbon source. These coatings facilitated the preservation of Co nanostructures at elevated temperatures which would damage the uncoated structures. The stabilization effect diminishes at temperatures higher than 500 °C, at which point nanopillars with the lower surface-to-

DOI: 10.1021/am506777a
ACS Appl. Mater. Interfaces 2015, 7, 2987−2992

volume ratio (i.e., the larger nanopillars) would be damaged because of the complete dissolution of the carbon film into the metal nanostructure. We show that this thermal stabilization is a general property of the carbon coating by demonstrating that titanium, which has very different properties from cobalt, is similarly protected against thermal deformation when coated with a carbon layer. Interestingly, because of the high reactivity of acetylene, graphitic coatings can be grown (though at higher temperatures) on nonmetallic substrates as well, such as Si/SiO_2 wafers[48] and nanowires,[49] so it is possible that a similar approach could also be used for the thermal stabilization of nonmetallic nanostructures.

■ ASSOCIATED CONTENT

Supporting Information

SEM images of annealed Co STFs, detailed experimental procedures, sample SEM images used for measuring width distribution, and SEM images of carbon-coated Co STFs annealed for 2 h. This material is available free of charge via the Internet at http://pubs.acs.org/.

■ AUTHOR INFORMATION

Corresponding Author

*E-mail: sinitskii@unl.edu.

Notes

The authors declare no competing financial interest.

■ ACKNOWLEDGMENTS

This work was supported by the Nebraska Center for Energy Sciences Research (#12-00-13), the Nebraska Research initiative, and the NSF through Nebraska MRSEC (DMR-1420645) and EPSCoR (EPS-1004094).

■ REFERENCES

(1) Du, X.; Skachko, I.; Barker, A.; andrei, E. Y. Approaching Ballistic Transport in Suspended Graphene. *Nat. Nanotechnol.* **2008**, *3*, 491−495.

(2) Bolotin, K. I.; Sikes, K. J.; Jiang, Z.; Klima, M.; Fudenberg, G.; Hone, J.; Kim, P.; Stormer, H. L. Ultrahigh Electron Mobility in Suspended Graphene. *Solid State Commun.* **2008**, *146*, 351−355.

(3) Mayorov, A. S.; Gorbachev, R. V.; Morozov, S. V.; Britnell, L.; Jalil, R.; Ponomarenko, L. A.; Blake, P.; Novoselov, K. S.; Watanabe, K.; Taniguchi, T.; Geim, A. K. Micrometer-Scale Ballistic Transport in Encapsulated Graphene at Room Temperature. *Nano Lett.* **2011**, *11*, 2396−2399.

(4) Balandin, A. A. Thermal Properties of Graphene and Nanostructured Carbon Materials. *Nat. Mater.* **2011**, *10*, 569−581.

(5) Lee, C.; Wei, X.; Kysar, J. W.; Hone, J. Measurement of the Elastic Properties and Intrinsic Strength of Monolayer Graphene. *Science* **2008**, *321*, 385−388.

(6) Nair, R. R.; Blake, P.; Grigorenko, A. N.; Novoselov, K. S.; Booth, T. J.; Stauber, T.; Peres, N. M. R.; Geim, A. K. Fine Structure Constant Defines Visual Transparency of Graphene. *Science* **2008**, *320*, 1308−1308.

(7) Bunch, J. S.; Verbridge, S. S.; Alden, J. S.; van der Zande, A. M.; Parpia, J. M.; Craighead, H. G.; Mceuen, P. L. Impermeable Atomic Membranes from Graphene Sheets. *Nano Lett.* **2008**, *8*, 2458−2462.

(8) Geim, A. K.; Novoselov, K. S. The Rise of Graphene. *Nat. Mater.* **2007**, *6*, 183−191.

(9) Novoselov, K. S.; Fal'ko, V. I.; Colombo, L.; Gellert, P. R.; Schwab, M. G.; Kim, K. A Roadmap for Graphene. *Nature* **2012**, *490*, 192−200.

(10) Lin, Y. M.; Dimitrakopoulos, C.; Jenkins, K. A.; Farmer, D. B.; Chiu, H. Y.; Grill, A.; Avouris, P. 100-Ghz Transistors from Wafer-Scale Epitaxial Graphene. *Science* **2010**, *327*, 662−662.

(11) Liao, L.; Lin, Y.-C.; Bao, M.; Cheng, R.; Bai, J.; Liu, Y.; Qu, Y.; Wang, K. L.; Huang, Y.; Duan, X. High-Speed Graphene Transistors with a Self-Aligned Nanowire Gate. *Nature* **2010**, *467*, 305−308.

(12) Wang, X.; Zhi, L.; Müllen, K. Transparent, Conductive Graphene Electrodes for Dye-Sensitized Solar Cells. *Nano Lett.* **2007**, *8*, 323−327.

(13) Bae, S.; Kim, H.; Lee, Y.; Xu, X. F.; Park, J. S.; Zheng, Y.; Balakrishnan, J.; Lei, T.; Kim, H. R.; Song, Y. I.; Kim, Y. J.; Kim, K. S.; Ozyilmaz, B.; Ahn, J. H.; Hong, B. H.; Iijima, S. Roll-to-Roll Production of 30-inch Graphene Films for Transparent Electrodes. *Nat. Nanotechnol.* **2010**, *5*, 574−578.

(14) Han, T.-H.; Lee, Y.; Choi, M.-R.; Woo, S.-H.; Bae, S.-H.; Hong, B. H.; Ahn, J.-H.; Lee, T.-W. Extremely Efficient Flexible Organic Light-Emitting Diodes with Modified Graphene Anode. *Nat. Photonics* **2012**, *6*, 105−110.

(15) Schedin, F.; Geim, A. K.; Morozov, S. V.; Hill, E. W.; Blake, P.; Katsnelson, M. I.; Novoselov, K. S. Detection of Individual Gas Molecules Adsorbed on Graphene. *Nat. Mater.* **2007**, *6*, 652−655.

(16) Lipatov, A.; Varezhnikov, A.; Wilson, P.; Sysoev, V.; Kolmakov, A.; Sinitskii, A. Highly Selective Gas Sensor Arrays Based on Thermally Reduced Graphene Oxide. *Nanoscale* **2013**, *5*, 5426−5434.

(17) Stoller, M. D.; Park, S.; Zhu, Y.; An, J.; Ruoff, R. S. Graphene-Based Ultracapacitors. *Nano Lett.* **2008**, *8*, 3498−3502.

(18) Yoo, E.; Kim, J.; Hosono, E.; Zhou, H.-S.; Kudo, T.; Honma, I. Large Reversible Li Storage of Graphene Nanosheet Families for Use in Rechargeable Lithium Ion Batteries. *Nano Lett.* **2008**, *8*, 2277−2282.

(19) Bunch, J. S.; van der Zande, A. M.; Verbridge, S. S.; Frank, I. W.; Tanenbaum, D. M.; Parpia, J. M.; Craighead, H. G.; Mceuen, P. L. Electromechanical Resonators from Graphene Sheets. *Science* **2007**, *315*, 490−493.

(20) Nair, R. R.; Blake, P.; Blake, J. R.; Zan, R.; Anissimova, S.; Bangert, U.; Golovanov, A. P.; Morozov, S. V.; Geim, A. K.; Novoselov, K. S.; Latychevskaia, T. Graphene as a Transparent Conductive Support for Studying Biological Molecules by Transmission Electron Microscopy. *Appl. Phys. Lett.* **2010**, *97*, 153102.

(21) Yuk, J. M.; Park, J.; Ercius, P.; Kim, K.; Hellebusch, D. J.; Crommie, M. F.; Lee, J. Y.; Zettl, A.; Alivisatos, A. P. High-Resolution EM of Colloidal Nanocrystal Growth Using Graphene Liquid Cells. *Science* **2012**, *336*, 61−64.

(22) Stoll, J. D.; Kolmakov, A. Electron Transparent Graphene Windows for Environmental Scanning Electron Microscopy in Liquids and Dense Gases. *Nanotechnology* **2012**, *23*, 505704.

(23) Kolmakov, A.; Dikin, D. A.; Cote, L. J.; Huang, J.; Abyaneh, M. K.; Amati, M.; Gregoratti, L.; Gunther, S.; Kiskinova, M. Graphene Oxide Windows for in Situ Environmental Cell Photoelectron Spectroscopy. *Nat. Nanotechnol.* **2011**, *6*, 651−657.

(24) Chen, S.; Brown, L.; Levendorf, M.; Cai, W.; Ju, S.-Y.; Edgeworth, J.; Li, X.; Magnuson, C. W.; Velamakanni, A.; Piner, R. D.; Kang, J.; Park, J.; Ruoff, R. S. Oxidation Resistance of Graphene-Coated Cu and Cu/Ni Alloy. *ACS Nano* **2011**, *5*, 1321−1327.

(25) Prasai, D.; Tuberquia, J. C.; Harl, R. R.; Jennings, G. K.; Bolotin, K. I. Graphene: Corrosion-Inhibiting Coating. *ACS Nano* **2012**, *6*, 1102−1108.

(26) Chen, Z. P.; Ren, W. C.; Gao, L. B.; Liu, B. L.; Pei, S. F.; Cheng, H. M. Three-Dimensional Flexible and Conductive Interconnected Graphene Networks Grown by Chemical Vapour Deposition. *Nat. Mater.* **2011**, *10*, 424−428.

(27) Bi, H.; Huang, F.; Liang, J.; Tang, Y.; Lu, X.; Xie, X.; Jiang, M. Large-Scale Preparation of Highly Conductive Three Dimensional Graphene and its Applications in CdTe Solar Cells. *J. Mater. Chem.* **2011**, *21*, 17366−17370.

(28) Kato, T.; Hatakeyama, R. Site- and Alignment-Controlled Growth of Graphene Nanoribbons from Nickel Nanobars. *Nat. Nanotechnol.* **2012**, *7*, 651−656.

(29) Wilson, P. M.; Mbah, G. N.; Smith, T. G.; Schmidt, D.; Lai, R. Y.; Hofmann, T.; Sinitskii, A. Three-Dimensional Periodic Graphene Nanostructures. *J. Mater. Chem. C* **2014**, *2*, 1879−1886.

DOI: 10.1021/am506777a
ACS Appl. Mater. Interfaces 2015, 7, 2987−2992

(30) Sun, J.; Simon, S. L. The Melting Behavior of Aluminum Nanoparticles. *Thermochim. Acta* **2007**, *463*, 32−40.
(31) Wronski, C. R. M. The Size Dependence of the Melting Point of Small Particles of Tin. *Br. J. Appl. Phys.* **1967**, *18*, 1731−1737.
(32) Buffat, P.; Borel, J. P. Size Effect on the Melting Temperature of Gold Particles. *Phys. Rev. A* **1976**, *13*, 2287−2298.
(33) Chookajorn, T.; Murdoch, H. A.; Schuh, C. A. Design of Stable Nanocrystalline Alloys. *Science* **2012**, *337*, 951−954.
(34) Cao, A.; Veser, G. Exceptional High-Temperature Stability Through Distillation-Like Self-Stabilization in Bimetallic Nanoparticles. *Nat. Mater.* **2010**, *9*, 75−81.
(35) Pan, X.; Fan, Z.; Chen, W.; Ding, Y.; Luo, H.; Bao, X. Enhanced Ethanol Production inside Carbon-Nanotube Reactors Containing Catalytic Particles. *Nat. Mater.* **2007**, *6*, 507−511.
(36) Joo, S. H.; Park, J. Y.; Tsung, C.-K.; Yamada, Y.; Yang, P.; Somorjai, G. A. Thermally Stable Pt/Mesoporous Silica Core-Shell Nanocatalysts for High-Temperature Reactions. *Nat. Mater.* **2009**, *8*, 126−131.
(37) Cao, A.; Lu, R.; Veser, G. Stabilizing Metal Nanoparticles for Heterogeneous Catalysis. *Phys. Chem. Chem. Phys.* **2010**, *12*, 13499−13510.
(38) Robbie, K.; Brett, M. J. Sculptured Thin Films and Glancing Angle Deposition: Growth Mechanics and Applications. *J. Vac. Sci. Technol., A* **1997**, *15*, 1460−1465.
(39) Hawkeye, M. M.; Brett, M. J. Optimized Colorimetric Photonic-Crystal Humidity Sensor Fabricated Using Glancing Angle Deposition. *Adv. Funct. Mater.* **2011**, *21*, 3652−3658.
(40) Kesapragada, S. V.; Victor, P.; Nalamasu, O.; Gall, D. Nanospring Pressure Sensors Grown by Glancing Angle Deposition. *Nano Lett.* **2006**, *6*, 854−857.
(41) Manera, M. G.; Montagna, G.; Ferreiro-Vila, E.; Gonzalez-Garcia, L.; Sanchez-Valencia, J. R.; Gonzalez-Elipe, A. R.; Cebollada, A.; Garcia-Martin, J. M.; Garcia-Martin, A.; Armelles, G.; Rella, R. Enhanced Gas Sensing Performance of TiO_2 Functionalized Magneto-Optical SPR Sensors. *J. Mater. Chem.* **2011**, *21*, 16049−16056.
(42) Schmidt, D.; Schubert, E.; Schubert, M. Optical Properties of Cobalt Slanted Columnar Thin Films Passivated by Atomic Layer Deposition. *Appl. Phys. Lett.* **2012**, *100*, 011912.
(43) Lai, S. L.; Carlsson, J. R. A.; Allen, L. H. Melting Point Depression of Al Clusters Generated During the Early Stages of Film Growth: Nanocalorimetry Measurements. *Appl. Phys. Lett.* **1998**, *72*, 1098−1100.
(44) Ramón, M. E.; Gupta, A.; Corbet, C.; Ferrer, D. A.; Movva, H. C. P.; Carpenter, G.; Colombo, L.; Bourianoff, G.; Doczy, M.; Akinwande, D.; Tutuc, E.; Banerjee, S. K. CMOS-Compatible Synthesis of Large-Area, High-Mobility Graphene by Chemical Vapor Deposition of Acetylene on Cobalt Thin Films. *ACS Nano* **2011**, *5*, 7198−7204.
(45) Weatherup, R. S.; Dlubak, B.; Hofmann, S. Kinetic Control of Catalytic CVD for High-Quality Graphene at Low Temperatures. *ACS Nano* **2012**, *6*, 9996−10003.
(46) Schmidt, D.; Kjerstad, A. C.; Hofmann, T.; Skomski, R.; Schubert, E.; Schubert, M. Optical, Structural, and Magnetic Properties of Cobalt Nanostructure Thin Films. *J. Appl. Phys.* **2009**, *105*, 113508.
(47) Booth, T. J.; Blake, P.; Nair, R. R.; Jiang, D.; Hill, E. W.; Bangert, U.; Bleloch, A.; Gass, M.; Novoselov, K. S.; Katsnelson, M. I.; Geim, A. K. Macroscopic Graphene Membranes and Their Extraordinary Stiffness. *Nano Lett.* **2008**, *8*, 2442−2446.
(48) Sinitskii, A.; Tour, J. M. Lithographic Graphitic Memories. *ACS Nano* **2009**, *3*, 2760−2766.
(49) Li, Y.; Sinitskii, A.; Tour, J. M. Electronic Two-Terminal Bistable Graphitic Memories. *Nat. Mater.* **2008**, *7*, 966−971.

DOI: 10.1021/am506777a
ACS Appl. Mater. Interfaces 2015, 7, 2987−2992